Properties of Langmuir and immobilized layers of betulin diphosphate on aqueous solutions of zinc sulfate and on the surface of zinc oxide nanoparticles

N. B. Melnikova,[a]★ D. S. Malygina,[b] O. A. Vorobyova,[b] A. G. Solovyeva,[b] K. L. Belyaeva,[b] D. V. Orekhov,[c] and A. V. Knyazev[a]

[a]*National Research Lobachevsky State University of Nizhny Novgorod, 23/5 prosp. Gagarina, 603950 Nizhny Novgorod, Russian Federation. Fax: +7 (831) 462 3085. E-mail: knyazevav@gmail.com*

[b]*Privolzhsky Research Medical University of the Ministry of Health of the Russian Federation, 10/1 pl. Minina i Pozharskogo, 603600 Nizhny Novgorod, Russian Federation. Fax: +7 (831) 439 0184. E-mail: melnikovanb@gmail.com*

[c]*Nizhny Novgorod State Technical University named after R. E. Alekseev, 24 ul. Minina, 603950 Nizhny Novgorod, Russian Federation. Fax: +7 (831) 436 9475. E-mail: mitriy07@mail.ru*

This work examines the specific features of interaction of betulin diphosphate (BDP), exhibiting antitumor and wound-healing properties, with zinc cations during its immobilization on ZnO nanoparticles. The properties of Langmuir and transferred BDP monolayers from an aqueous subphase of zinc sulfate onto the surface of a solid substrate (CaF_2, quartz) by the Langmuir—Schaefer method are investigated using IR and UV spectroscopy. It is shown that there is a twofold increase of the molecular area in the immobilized layers, while the compressibility modulus decreases by a factor of 1.5. Zinc oxide nanoparticles with immobilized BDP 10—20 nm in size (surface concentration of BDP is 100 mg g^{-1}) retain the original hexagonal wurtzite structure. The efficiency of betulin diphosphate immobilized on the surface of zinc oxide nanoparticles is demonstrated in *in vivo* experiments for burn wounds in rats.

Key words: betulin diphosphate, immobilization, zinc oxide nanoparticles, Langmuir monolayers.

Interest toward betulin (lup-20(29)-ene-3β,28-diol), a component of birch bark (*Betula pendula*), and its natural and synthetic derivatives is due to antitumor, hepatoprotective, antiviral, and other pharmacological properties of these compounds.[1—5] Their main disadvantage is extremely low solubility in water, which reduces bioavailability and requires additional delivery systems: either in the form of conjugates of these compounds or inclusion complexes with various polymers and oligomers, or their introduction into nanocontainers (liposomes, niosomes, micelles, *etc.*).[6—14]

A common technique for increasing the bioavailability of triterpenoids is to obtain their phosphate and phosphonate derivatives since phosphates are involved in most metabolic processes in the human body.[15,16] The important advantages of phosphate-containing molecules include their high ability to interact with amines, amino acids, protein NH_2 and NH groups through the formation of covalent and hydrogen bonds or as a result of non-covalent binding. For example, dexamethasone sodium phosphate (CAS 55203-24-2) ([2-[(8*S*,9*R*,10*S*,11*S*,13*S*,14*S*,16*R*,17*R*)-9-fluoro-11,17-dihydroxy-10,13,16-trimethyl-3-oxo-6,7,8,11,12,14,15,16-octahydrocyclopenta[*a*]phenanthrene-17-yl]-2-oxoethyl]phosphate disodium salt), in contrast to the initial steroid, is readily soluble in water.[17]

In *in vivo* experiments on mice and rats, 3,28-betulin diphosphate (BDP) demonstrated antioxidant and wound-healing properties, as well as antitumor activity against grafted Ehrlich ascites carcinoma.[18,19] We note that its solubility is almost 10^4 times higher than that of betulin (B).[20]

Previously, the ability of metal nanoparticles to induce apoptosis in tumor cells and death of bacterial cells due to the generation of reactive oxygen species (ROS) was demonstrated.[21—23] It is known that the immobilization of betulin and betulinic acid on the surface of silver and gold nanoparticles led to an increase of their efficiency against various types of melanoma.[24,25] Therefore, we expected to see an increase in the antitumor properties and anti-inflammatory activity of BDP upon its immobilization on the surface of metal nanoparticles, which contribute to the death of bacterial and tumor cells.

Published in Russian in *Izvestiya Akademii Nauk. Seriya Khimicheskaya,* No. 2, pp. 289—300, February, 2021.

1066-5285/21/7002-0289

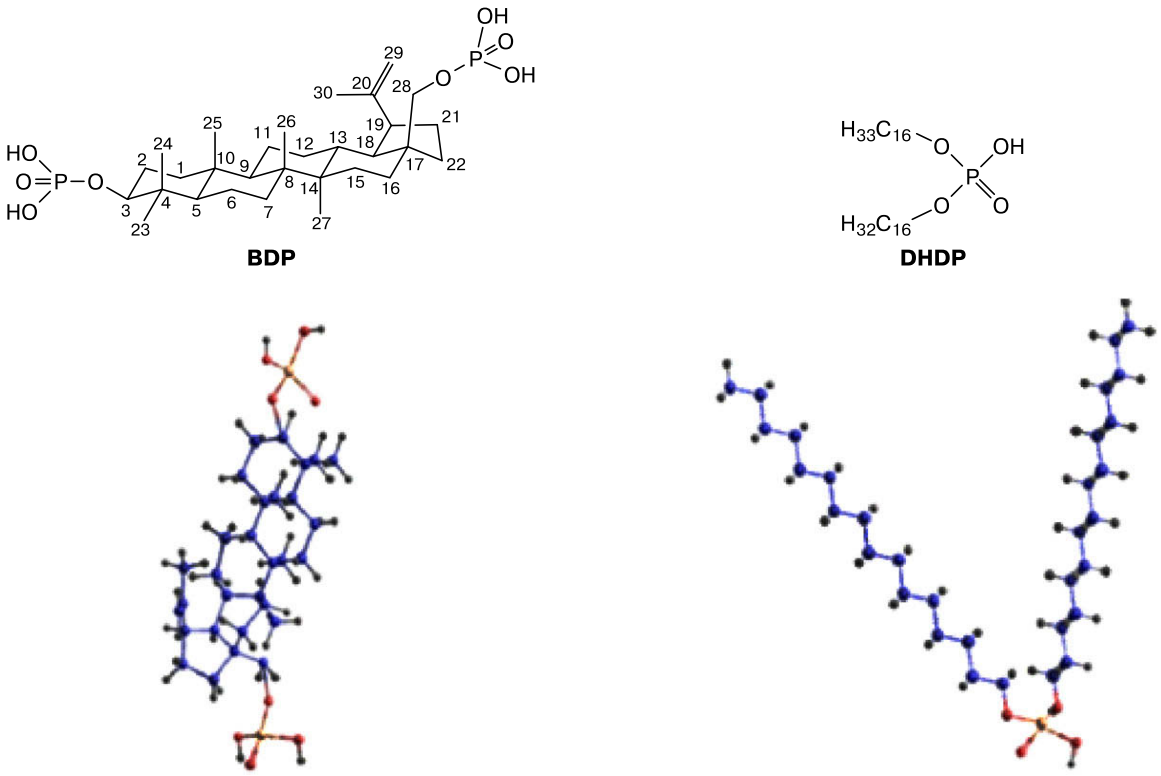

Fig. 1. Structures of betulin diphosphate (*a*) and dihexadecyl phosphate (*b*).

Among metal-containing nanoparticles, semiconducting zinc oxide nanoparticles are of particular interest, due to the biogenicity of zinc cations. They are part of or control the action of nearly three hundred enzymes, which are involved in various biochemical processes in the human body. The advantages of zinc oxide nanoparticles include lower toxicity (LD_{50} > 8000 mg kg^{-1}, rats, orally)[26] compared to gold (LD_{50} > 2000 mg kg^{-1}) and silver nanoparticles (LD_{50} > 4000 mg kg^{-1}),[27,28] as well as the ability to exhibit the properties of quantum dots, which allows them to be used in theranostics due to the enhancement of antitumor and antibacterial effects.[29,30]

This work is devoted to the preparation and study of the properties of zinc nanoparticles modified by BDP. For this purpose, the interaction of BDP with zinc cations in the subphase of an aqueous solution of $ZnSO_4$ and on the surface of zinc oxide nanoparticles, the physicochemical properties of ZnO nanoparticles were studied, and the biological activity of modified zinc oxide nanoparticles was demonstrated for a model of a burn wound in rats.

Experimental

Materials and reagents. We used commercially available reagents without additional purification: betulin (lup-20(29)-ene-3α,β,28-diol, $C_{30}H_{50}O_2$, Sigma-Aldrich, CAS 473-98-3), dihexadecyl phosphate (DHDP) (Sigma-Aldrich, CAS 2197-63-9), 96% ethanol (C_2H_5OH, GOST 51652-2000), zinc acetate $Zn(CH_3COO)_2 \cdot 2H_2O$ (GOST 5823-78), acetonitrile (Kriokhrom, TU 2634-002-54260861-2013, Grade 0), deionized water (FS 42-0324-09, Elix 3, cartridge Progard Millipore, France) with a specific resistance of less than 0.2 μS at a temperature of 20±10 °C and pH 5.5, zinc sulfate $ZnSO_4 \cdot 7H_2O$ (GOST 4174-77), calcium acetate $Ca(CH_3COO)_2$ (GOST 3159-76), sodium hydroxide NaOH (GOST 4328-77), sunflower oil, refined, deodorized. Betulin diphosphate (lup-20(29)-ene-3α,β,28-diphosphate) was obtained in accordance with the previously described procedure.[19] The structures of BDP and DHDP are shown in Fig. 1.

Preparation of zinc oxide nanoparticles.[31,32] We used freshly prepared methanolic solutions, specifically, a 2% sodium hydroxide solution and a 1.5% zinc acetate solution at 70 °C. A NaOH solution (10 mL) was added dropwise to a zinc acetate solution (30 mL) while cooling in an ice bath and stirring for 5—10 min. The white flakes formed throughout the bulk were precipitated with heptane (60 mL). After the separation of liquid and solid phases, heptane (50 mL) was added to the filtrate for a more thorough precipitation of ZnO nanoparticles. The resulting precipitate was washed on a paper filter with ethanol, then dried for 5 h at 105±5 °C in a drying oven and placed in a desiccator for further storage.

Langmuir monolayers and films. A KSV Nima device (Finland) was used for the formation of Langmuir monolayers. Compression isotherms of monolayers were recorded using an automated Langmuir balance with a platinum Wilhelmy measuring plate at a constant temperature. Betulin diphosphate (concentration 1.0 mg mL^{-1}) was dissolved in a chloroform—ethanol

mixture (5 : 1 v/v), then the solution (20 μL) was applied to the surface of the subphase (water) dropwise using a microsyringe for 30—40 min. The surface pressure was

$$\pi = \gamma_0 - \gamma,$$

where γ_0 and γ are the subphase surface tension before and after applying the monolayer, mN m^{-1}. Area (S_0) per monolayer molecule was determined graphically by extrapolating the downward sloped section at the intersection point of the section of the $\pi = f(S)$ isotherm onto the abscissa axis to $\pi = 0$. The compressibility modulus (C_S^{-1}, mN m^{-1}), used for the characterization of the phase state of the monolayers, was calculated by the formula

$$C_S^{-1} = -S_0(d\pi/dS)_{P,T}.$$

Deionized water; $1 \cdot 10^{-3}$ mol L^{-1} aqueous solutions of $Ca(OAc)_2$; and $1 \cdot 10^{-4}$, $1 \cdot 10^{-3}$, and $1 \cdot 10^{-2}$ mol L^{-1} aqueous solutions of $ZnSO_4$ were used as a subphase.

Thin films on quartz and on CaF_2 were formed according to the Langmuir—Schaefer method by transfer from the water surface.

Physical and chemical studies. The structure of the films was studied on a Shimadzu XRD-6000 X-ray diffractometer (Japan) at 295(2) K (Cu-Kα radiation, λ = 1.5418 Å, Bragg-Brentano reflection geometry) in the range of incidence angles 2θ = 5—50° with a step of 0.026° and a scanning rate of 0.067335 deg s^{-1}. The X-ray diffraction patterns of the amorphous samples have diffraction peaks at 37.5° and 44.0°, which are related to the material of the cell. Sample fluorescence spectra were recorded on an RF-600 Shimadzu spectrofluorimeter (Japan) under excitation with light (λ = 320 nm) in the wavelength range 350—800 nm using a cell with a thickness of 10 mm. IR spectra were recorded on an IR Prestige-21 FTIR spectrophotometer (Shimadzu, Japan) in the wavelength range 4000—400 cm^{-1} using tablets with KBr. Chromatograms were obtained on an automatic high performance liquid chromatograph LC-20Avp (Shimadzu, Japan) in a reversed phase mode (RP-HPLC) with a mobile phase degasser, a column thermostat, and diode-array UV detection at 196 and 210 nm, a Discovery C18 column (5 μm, Supelco, 25 cm×4.6 mm), column temperature 40±1 °C. An acetonitrile—deionized water mixture (9 : 1 v/v) was used as the eluent, the flow rate was 1.0 mL min^{-1}, the volume of the injected sample was 20 μL, and the chromatogram recording duration was 20 min. Electronic spectra were recorded on a UV-1800 UV-Vis spectrophotometer (Shimadzu, Japan) in the wavelength range 220—280 nm; the cell material was quartz, cell thickness was 10 mm.

Biological experiment. The studies were carried out on white Wistar rats (Stolbovaya branch, Scientific Center for Biomedical Technologies, Russian Federation), kept in accordance with the rules of the European Convention ET/S 129 (1986) and directive 86/609 ESC. The study was approved by the Local ethics committee No. 1 of the Privolzhsky Research Medical University of the Ministry of Health of the Russian Federation, protocol No. 16 dated 02.12.2016.

The blood of white Wistar rats stabilized with sodium citrate (the ratio of blood to sodium citrate solution was 1 : 9 v/v) was used to study antioxidant activity. Solutions of betulin derivatives and their mixtures with antitumor substances in ratios 1 : 2; 1 : 5; 1 : 10 (v/v) were added to rat whole blood. Erythrocytes were washed twice in 0.9% NaCl solution by centrifugation for 10 min at 1600*g*. The intensity of lipid peroxidation in plasma and erythrocytes was determined by the content of the secondary product of free radical oxidation, namely, malondialdehyde, following the established procedure described in the work.[33] Superoxide dismutase (SOD) activity (EC 1.15.1.1) was determined in the hemolysate of washed erythrocytes (1 : 10 v/v) using the inhibition of the formation of the adrenaline autooxidation product.[34] The activity of catalase[35] (EC 1.11.1.6) and glutathione reductase[36] (EC 1.8.1.7) was determined spectrophotometrically using previously described procedures.

Experimental *in vivo* studies were carried out in accordance with regulation documents[37] on 10 male Wistar rats weighing 200±2.6 g. The modeling of a grade IIIb skin burn (7% of the total body surface) was carried out by applying dosed burns with an area of 235 mm^2 (3×78.5 mm^2) to the depilated skin of the lumbar region of rats, the temperature of the burn surface was about 300 °C and the duration of contact with the skin was 1 s. Prior to this procedure, nembutal anesthesia was administered with a dose of 35—40 mg kg^{-1}. When modeling the burn wound, the general state of the animals and the healing rate of the wound surface were recorded. The efficiency of oleogel action (dose 10 mg cm^{-2}) was investigated in three groups. In the control group, considered as 100%, the thermal burn was applied without treatment; in the first group, the treatment was carried out with sunflower oil; in the second group, the treatment used oleogel based on zinc oxide nanoparticles modified with BDP and betulin; in the third group, the treatment involved methyluracil ointment.

Statistical processing was carried out using Microsoft Excel.

Results and Discussion

Properties of monolayers on an aqueous subphase. The intermolecular interactions between zinc cations and BDP were evaluated using BDP Langmuir monolayers on an aqueous subphase containing zinc sulfate solutions (BDP monolayers on deionized water were used for a comparison). The surface pressure isotherms $\pi = f(S)$ at a constant temperature for the obtained monolayers of BDP and dihexadecyl phosphate on various subphases are shown in Fig. 2.

Betulin diphosphate forms stable monolayers on water, characterized by a molecular area $S_0 = 0.41 \pm 0.02$ nm^2 molecule^{-1} (Fig. 2, *a*, curve *1*, Table 1). The solubility of BDP and other betulin derivatives in water and in organic solvents depends on the polymorphic form of triterpenoids, but does not affect the state of the monolayers obtained by applying chloroform—ethanol solutions of triterpenoids. The molecular area S_0 of the polar anionic surfactant BDP in a monolayer on a pure water subphase is similar to the value characteristic for non-polar triterpene alcohols, namely cholesterol and lupeol (S_0 = = 0.40±0.03 nm^2 molecule^{-1}).[38,39] Grafting of the polar part to the cholesterol skeleton in the form of a hemisuccinate leads to the formation of monolayers on water, the state of which is characterized by at least two phase transitions: in the region of surface pressures up to 15—20 mN m^{-1} (S_0 = 0.50—0.52 nm^2 molecule^{-1}), and in the range

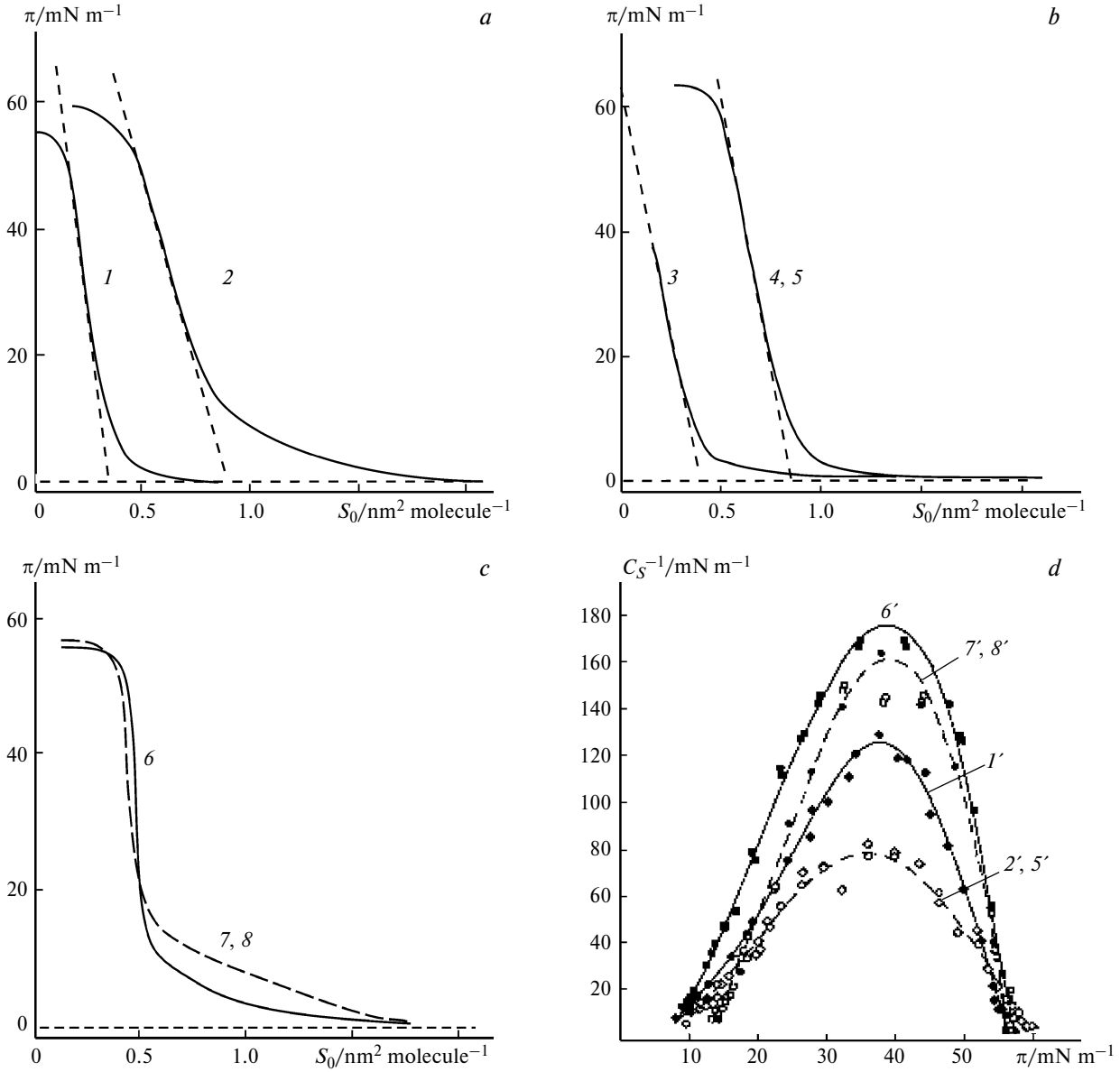

Fig. 2. Compression isotherms (π—*S*-isotherms) of Langmuir monolayers of betulin diphosphate (*a, b*) and dihexadecyl phosphate (*c*) on water and on aqueous subphases; dependence of the compressibility modulus on surface pressure $C_S^{-1} = f((\pi)$ (*d*) (see Table 1 for designations).

20—40 mN m^{-1} with S_0 = 0.33—0.44 nm^2 molecule^{-1}.[40] A S_0 value equal to 0.40±0.05 nm^2 molecule^{-1} determines the theoretically calculated molecular area of triterpenoids in a densely packed monolayer for a perpendicular orientation.[41] An increase of the molecular area of betulinic acid and betulin in a monolayer to 0.67 and 0.50 nm^2 molecule^{-1}, respectively, was explained by the authors of the work[42] by the ability of betulinic acid to occupy both perpendicular and oblique positions in a monolayer, or to form bilayer structures.

Monolayers of BDP formed on the subphase of aqueous solutions of salts of divalent biogenic cations (calcium acetate and zinc sulfate) are characterized by a twofold increase of the molecular area to 0.87±0.02 nm^2 molecule^{-1} compared to BDP monolayers on water, with this value being dependent on electrolyte concentration in the subphase (see Fig. 2, *a*, *b*).

The influence of polar phosphate groups in BDP, which has a large hydrophobic fragment in the triterpene skeleton, on the interaction with zinc cations at the interface was studied using monolayers of the well-known and stable dihexadecyl phosphate.

In contrast to lecithin phosphate-containing derivatives and unstable derivatives of betulin monophosphates, surfactant DHDP on an aqueous zinc sulfate subphase forms

Table 1. Characteristics of BDP and DHDP monolayers on the surface of aqueous solutions (for Fig. 2)*

Curve	Monolayer	Subphase	S_0/nm^2 molecule^{-1}	C_S^{-1}/mN m^{-1}
1, *1′*	BDP	H_2O	0.40±0.02	120±3
2, *2′*	BDP	$1\cdot10^{-3}$ mol L^{-1} aqueous solution of $Ca(OAc)_2$	0.87±0.02	80±5
3	BDP	$1\cdot10^{-4}$ mol L^{-1} aqueous solution of $ZnSO_4$	0.42±0.02	—
4	BDP	$1\cdot10^{-2}$ mol L^{-1} aqueous solution of $ZnSO_4$	0.87±0.03	—
5, *5′*	BDP	$1\cdot10^{-3}$ mol L^{-1} aqueous solution of $ZnSO_4$	0.87±0.03	80±5
6, *6′*	DHDP	H_2O	0.50±0.02	180±3
7, *7′*	DHDP	$1\cdot10^{-3}$ mol L^{-1} aqueous solution of $ZnSO_4$	0.49±0.02	160±3
8, *8′*	DHDP	$1\cdot10^{-3}$ mol L^{-1} aqueous solution of $Ca(OAc)_2$	0.49±0.02	155±5

* Three repetitions.

stable reproducible layers that are convenient for comparison with BDP monolayers.

Earlier in the works[43,44] when studying the surface layers of DHDP, a phosphate group proton was proven to participate in reactions with cations (for example, sodium and lanthanides) in metal salt solutions, leading not only to physical, but also to specific adsorption due to chemical interactions, which in turn causes the repulsion or attraction of ions in the surface layers. The interactions at the DHDP film—metal salt solution interface were observed at a pH ~5—6 for the liquid phase of the monolayer with a surface pressure of less than 10—15 mN m^{-1}.

The differences in the character of π—*S*-compression isotherms of DHDP and BDP monolayers on aqueous zinc salt solutions at pH 5.5 in the liquid-condensed or solid phase region of the film makes it possible to evaluate the effect of zinc ions on the properties of monolayers of these phosphates.

The appearance of surface pressure isotherms $\pi = f(S)$ of DHDP monolayers at $\pi > 15$ mN m^{-1} and the molecular area S_0 in the DHDP monolayer were practically independent of the nature of the components in an aqueous subphase, S_0 corresponded to 0.49±0.02 nm^2 molecule^{-1} (see Fig. 2, *c*, Table 1). Similar molecular area values for DHDP in monolayers were obtained on an aqueous subphase of a 0.01 *M* $AgNO_3$ solution (0.46 nm^2 molecule^{-1})[45] and on an aqueous subphase of a 0.1 *M* NaCl solution.[35]

The analysis of the dependence of the compressibility modulus on surface pressure $C_S^{-1} = f(\pi)$ allows us to consider the state of BDP and DHDP monolayers on an electrolyte subphase, as well as DHDP monolayers on pure water as a liquid-condensed phase (C_S^{-1} = = 160—180 mN m^{-1}). Betulin diphosphate and betulinic acid[42] have polar groups at the ends of the molecule and form monolayers on pure water, which are characterized by lower values of the compressibility modulus (110—120 mN m^{-1}) (see Table 1, Fig. 2, *d*), in contrast to lupeol, which forms more rigid films (250 mN m^{-1}).

Thus, in contrast to BDP, the properties of DHDP monolayers on an aqueous subphase of a zinc sulfate solution and water are practically the same (similar molecular areas, insignificant changes in C_S^{-1}), which can be explained by the strictly vertical orientation of DHDP molecules in a densely packed monolayer, where there is a weak effect of the immobilized (or adsorbed) zinc cation on the parameters of monolayer compression isotherms in the region $\pi > 10$—15 mN m^{-1}.

The expected scheme of interaction of zinc cations in a subphase with BDP, which has four nonequivalent hydroxyl protons in phosphate groups, is probably more complex. The BDP molecules are able to not only "submerge" into the subphase at the spreading stage and occupy various positions in a monolayer on water, but also form bilayer structures, similar to lecithins (Fig. 3, *a*, *b*, *c*). The structure of the BDP monolayer at the air—electrolyte solution interface is influenced by many factors, such as ionization of BDP phosphate groups, hydrophobic binding of the BDP triterpene skeleton, and the possibility of formation of hydrogen bonds and various zinc salt complexes. Similar specific features of interaction were observed for cholesterol hemisuccinate monolayers on a calcium phosphate subphase.[38] Oleanolic acid, cholesterol, cholesterol hemisuccinate can form an oblique or bilayer structure.[38,46] A "face-on" orientation of BDP molecules at the interface is not excluded (Fig. 3, *d*), similar to tetrapyridylporphyrin molecules in monolayers on the surface of zinc and copper salts.[47]

The effect of four nonequivalent BDP protons on the interaction with $ZnSO_4$ in an aqueous subphase was studied using mixed monolayers of BDP and DHDP. The latter contains a single hydroxyl proton, its molecules have a low sensitivity toward the action of zinc cations and do not change their perpendicular orientation in a densely packed monolayer (Fig. 4, *a*, *b*).

In an ideal mixed monolayer of BDP and DHDP, the theoretical molecular area of each of the components can be calculated using the additivity principle:

$$S_t = x_1 S_1 + (1 - x_1) S_2,$$

where x_1 is the molar fraction of BDP; $(1 - x_1)$ is the molar fraction of DHDP; S_1, S_2 are the molecular areas of BDP

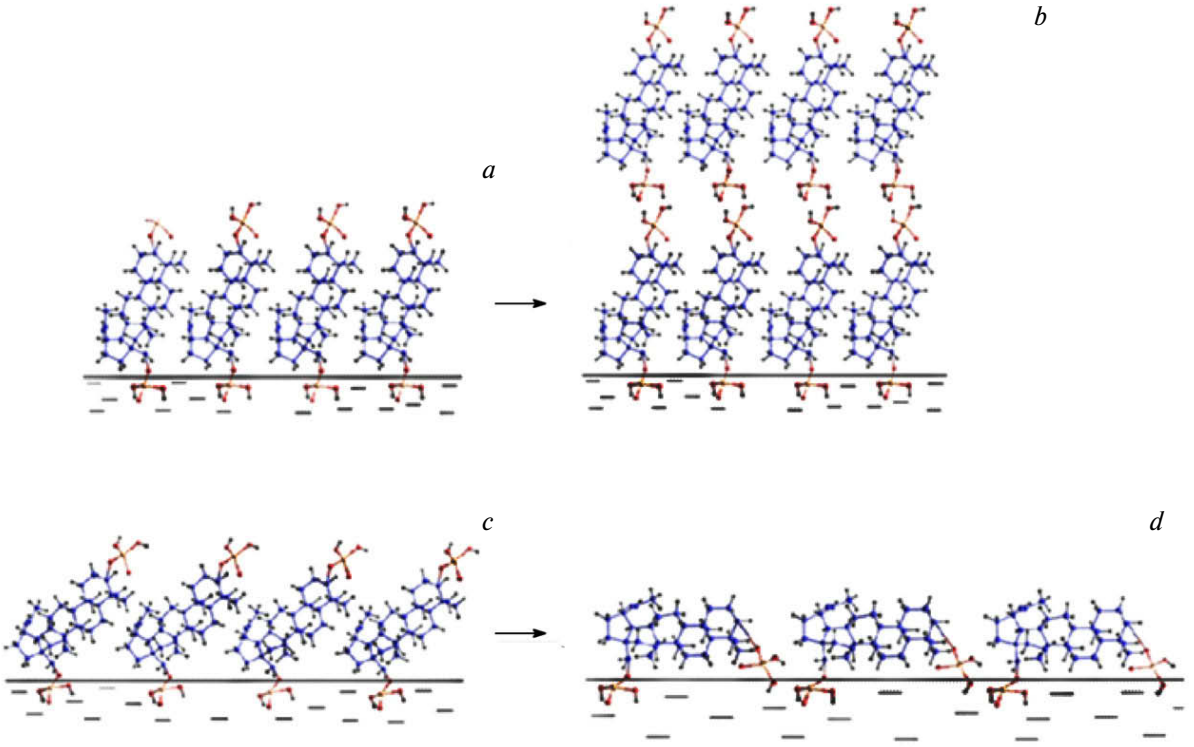

Fig. 3. Possible arrangement of BDP molecules at the air—subphase interface for a surface pressure above 15 mN m^{-1}; *a*, vertical orientation; *b*, formation of bilayer structures; *c*, oblique orientation; *d*, "face-on" orientation.

and DHDP, respectively, in monolayers of individual substances on an aqueous $ZnSO_4$ subphase.

Thus, the experimental molecular area in mixed monolayers of porphyrin fluorophore and naphthalimide, which had no chemical interactions between their molecules, corresponded to calculations based on the additivity principle.[48]

Considerable deviations between experimental and calculated results are observed in the region of condensed monolayers with a molar fraction of BDP ranging from

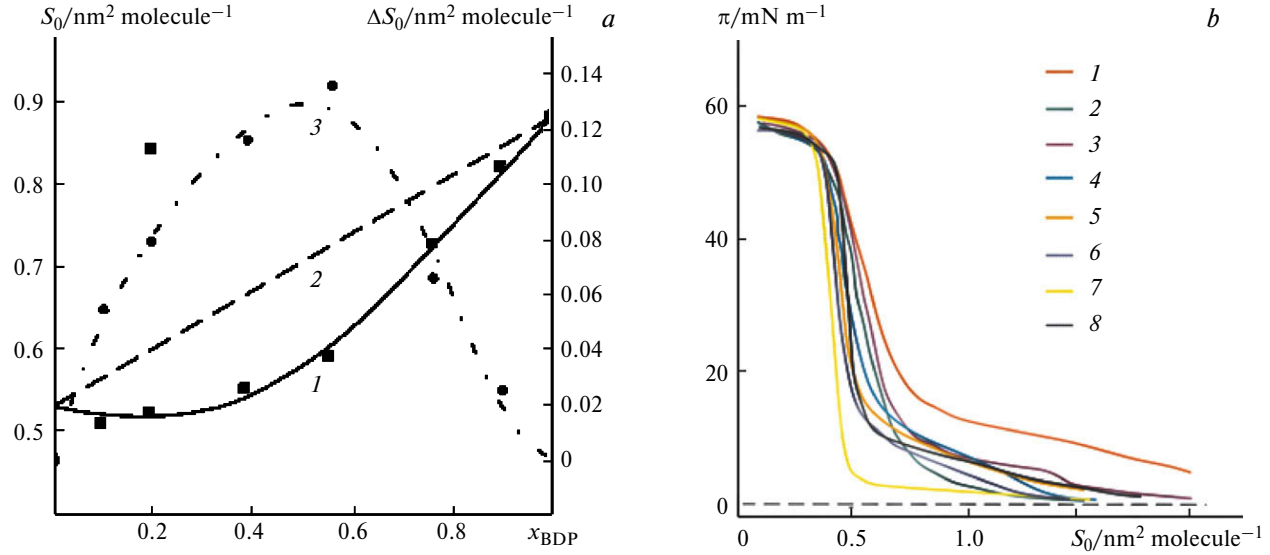

Fig. 4. Dependencies of the molecular area (S_0) on molar fraction of BDP (x_{BDP}) in mixed monolayers of BDP and DHDP on a zinc sulfate subphase; *1* is the experiment (S_0^{exp}), *2* is the calculation (S_0^{theor}), *3* is the dependence $\Delta S_0 = S_0^{theor} - S_0^{exp}$ (*a*); compression isotherms $\pi = f(S)$ of mixed monolayers (*b*); x_{BDP}: 1.00 (*1*), 0.90 (*2*), 0.76 (*3*), 0.56 (*4*), 0.39 (*5*), 0.20 (*6*), 0.10 (*7*), 0 (*8*).
Note. Figure 4 is available in full color on the web page of the journal (https://link.springer.com/journal/volumesAndIssues/11172).

0.3 to 0.6 in Fig. 4, *a*, which indicates that the BDP structure has a considerable effect on the state of mixed BDP—DHDP monolayers. The considerable influence of intermolecular interactions on the state of mixed films is most noticeable in the region of liquid-stretched films, $\pi = 0—15$ mN m^{-1} (Fig. 4, *b*). Additional information on the formation of surface salt complexes can be obtained by analyzing the IR spectra of BDP monolayers (20 monolayers) transferred from an aqueous subphase of a 0.01 *M* zinc sulfate solution to a solid substrate surface by the Langmuir—Schaefer method. The IR spectra of the starting BDP and the transferred BDP—Zn^{2+} monolayers retain the bands of stretching vibrations of the triterpene skeleton (2942—2871 cm^{-1}), hydroxyl groups in the region of 3364 cm^{-1}, a complex combined band (ν_{comb}) of bending and stretching vibrations of the O=P—O—H group and water in the range 1650—1620 cm^{-1}. The complex bands of stretching vibrations ν(C—O) and ν(P—O) in the range 1200—950 cm^{-1} undergo slight changes. The band observed at 1033 cm^{-1} in the starting BDP spectrum split into several bands, specifically, 1018, 1057, 1106, and 1129 cm^{-1}, in the spectrum of transferred monolayers. The greatest changes were observed in the spectral region characteristic for bending vibrations δ(O—P—O). The band in the region of 501 cm^{-1} of the starting BDP spectrum considerably changed its shape and position; the vibrations δ(O—P—O) appeared in the range 604—517 cm^{-1}. Taking into account that zinc-phytate complexes, which have a similar nature of binding of zinc to the phosphate group in organic compounds, are characterized by δ(O—P—O) vibrations of the phosphate group in the region of 541.5±2.0 cm^{-1} and vibrations of the C—O—P group in the region of 993.5±4.0 cm^{-1}, it can be assumed that the structure of the transferred BDP—Zn^{2+} layers corresponds to salt complexes.[49]

The formation of salt complexes BDP—Zn^{2+} at the BDP monolayer—aqueous solution of Zn^{2+} interface can be a convenient method for grafting BDP onto the surface of zinc oxide nanoparticles (ZnONP). Usually, the immobilization of betulin and betulinic acid on the surface of gold and silver nanoparticles involves complex modification of the nanoparticle surface, for example, conjugation with thiols or PEGylation, which allows the nanoparticles to act as a delivery vector for triterpenoids.[24,25] The preparation of BDP—Zn^{2+} complexes on the zinc oxide nanoparticle surface makes it possible to not only solve the problem of transported delivery of the triterpenoid, but also of the stabilization of zinc oxide nanoparticles in the H^+-form.[50,51] In comparison with ZnO, these protonated particles interact more efficiently with negatively charged phospholipids on the outer membrane of the cell, are absorbed by it, and release zinc cations, which ultimately leads to the generation of oxygen active species and, subsequently, to apoptosis of tumor cells.

Immobilization of betulin diphosphate on the surface of zinc oxide nanoparticles. The immobilization of BDP on zinc oxide nanoparticle surface was carried out by sorption from a $1 \cdot 10^{-3}$ *M* ethanolic solution of BDP for 30—60 min. The sorption process was monitored independently by UV spectroscopy of a complex band of absorption of phosphate groups in the range 252—258 nm (Fig. 5), as well as by RP-HPLC. Preliminarily, a linear dependence of absorption (*A*) at 256 nm in an ethanolic solution of BDP on concentration was established (Fig. 5, *a*). The studies took into account the absorption of the obtained zinc oxide nanoparticles in the UV range 350—370 nm, which characterizes the semiconductor nanoparticle band gap (Fig. 5, *c*).

It can be assumed that BDP, similar to metabolically important derivatives of phosphoric acid (glucose-1-phosphate, glucose-6-phosphate, inosine-mono-, -di-, and -triphosphates, pyridoxal phosphate), both in a biological environment and during the modification of zinc oxide nanoparticles, reacts with the transfer of one or two protons. Most likely, BDP with ionized phosphate groups forms salt chelate structures on the surface of zinc oxide nanoparticles.

The effect of ionization of BDP during adsorption from ethanolic solution on freshly prepared zinc oxide nanoparticles was reflected in the change of absorption A^{256} over time for 30 min (Fig. 6, *a* and *b*). The concentration of BDP after 3 h of adsorption, taking into account the absorption of zinc oxide nanoparticles in the range 252—258 nm, reached 95—130 mg g^{-1}. The A^{256} values were close to those of the plateau after 3 h, while the surface concentration of BDP (Γ) according to HPLC-analysis with a phosphate buffered saline eluent (pH 6.8), in which the ionized state of BDP remains unchanged, reaches the plateau after 40 min (Fig. 6, *c*). Therefore hereinafter, the surface concentration of BDP is taken to be 100 mg g^{-1}, calculated by HPLC 30—40 min after the beginning of adsorption.

Powder X-ray diffraction showed that the structure of zinc oxide nanoparticles with immobilized BDP, as well as of the starting nanoparticles, is a crystalline form of wurtzite (Fig. 7, *a*, *b*).[52]

The average sizes of zinc oxide nanoparticles (diameter), calculated in accordance with the Scherrer formula

$$D = 0.89\lambda/(\beta\cos\theta),$$

where 0.89 is dimensionless particle shape factor; λ is the wavelength of X-ray radiation; β is the reflex linewidth at half height in rad; θ is scattering angle in rad, are given in Table 2.

Thus, the average size of zinc oxide nanoparticles and particles with immobilized BDP (ZnONP—BDP) was 17.8 and 11.7 nm, respectively.

The IR spectra of the starting zinc oxide nanoparticles had an absorption band at 450 cm^{-1}, which is character-

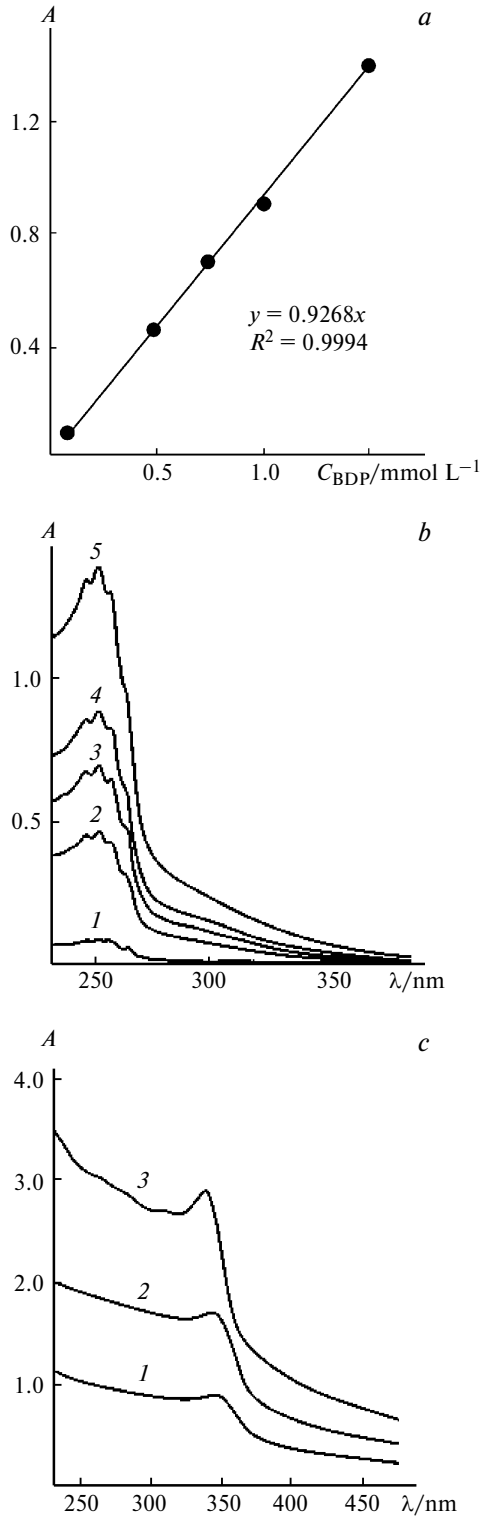

Fig. 5. Concentration dependence of the absorption (*A*) of an ethanolic solution of BDP at 256 nm (*a*); UV spectra of ethanolic solutions of BDP (*b*) and ZnONP dispersions (*c*) at various concentrations; reference solution is C_2H_5OH; *b* is concentration of BDP (mmol L^{-1}): 0.05 (*1*), 0.5 (*2*), 0.75 (*3*), 1.0 (*4*), 1.5 (*5*); *c* is concentration of ZnONP dispersions (mmol L^{-1}): 1.67 (*1*), 3.34 (*2*), 6.68 (*3*).

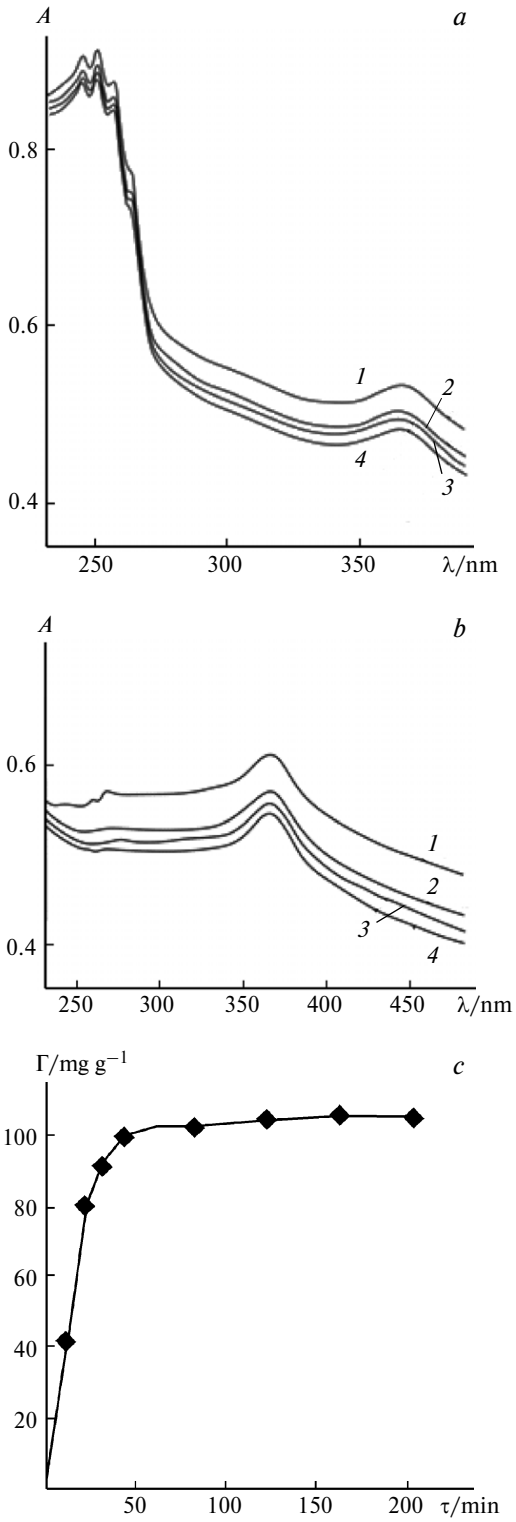

Fig. 6. Dynamics of changes in the absorption of dispersions of ZnONP—BDP in C_2H_5OH at λ_{max} = 256 nm for 0—30 min with an interval of 10 min (*1*—*4*) (C_{BDP} = 1.34 mmol L^{-1}, C_{ZnONP} = = 3.34 mmol L^{-1}) (*a*, *b*); reference solution is C_2H_5OH (*a*) and an ethanolic solution of BDP (C_{BDP} = 1.34 mmol L^{-1}) (*b*); dependence of BDP surface concentration (Γ) on time according to HPLC (eluent is phosphate buffer pH 6.8) (*c*).

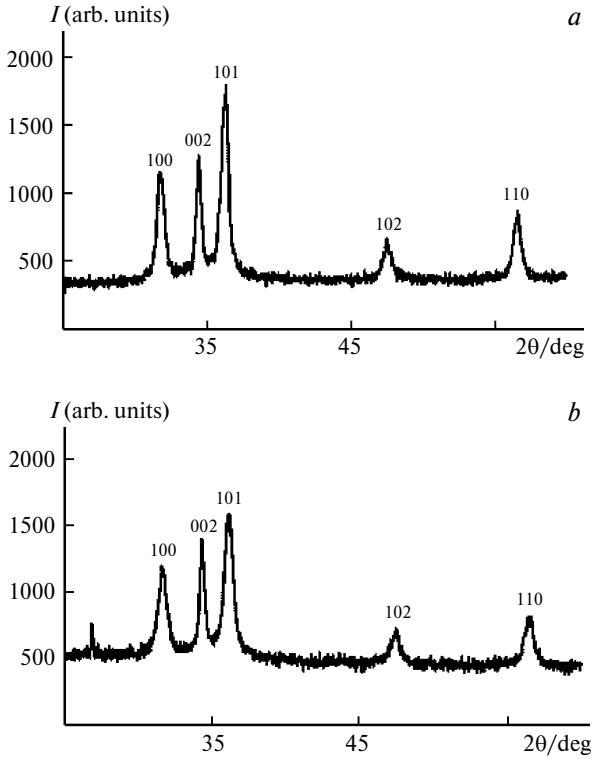

Fig. 7. X-ray diffraction patterns of ZnONP (*a*) and ZnONP—BDP (*b*).

istic of zinc oxide nanoparticles,[53—58] and absorption bands of OH groups of adsorbed solvents (ethanol and water) at 3396 cm^{-1}. The IR spectrum of zinc oxide nanoparticles with immobilized BDP, similar to the spectrum of transferred betulin diphosphate monolayers, contained bands of stretching vibration of the BDP hydrocarbon skeleton (CH, CH_2, CH_3) in the region of 2943 and 2872 cm^{-1} and strong bands in the range 1200—900 cm^{-1}, characteristic of stretching vibrations ν(P—O) (1215—1192 cm^{-1}) and ν(C—O) (1033—900 cm^{-1}).

To study the effect of immobilized betulin diphosphate (ZnONP—BDP) on nanoparticle fluorescence, we studied the fluorescence of zinc oxide nanoparticles with immobilized betulin (ZnONP—B) in an ethanolic solution

Table 2. X-ray diffraction results (for Fig. 7)*

Peak	ZnONP (*a*)			ZnONP—BDP (*b*)		
	101	102	110	100	002	101
β′, 2θ	0.468	0.545	0.625	0.714	0.476	0.714
β/rad	0.0082	0.0082	0.0109	0.0125	0.0083	0.0125
2θ/deg	36.22	47.54	56.62	31.76	34.36	36.22
cosθ	0.950	0.911	0.878	0.959	0.954	0.950
D/nm	17.8	16.0	14.5	11.6	17.5	11.7

* β′ is reflex linewidth at half height, 2θ; β is reflex linewidth at half height, rad; 2θ is Bragg scattering angle/deg.

(Fig. 8, *a*), as well as the fluorescence of the starting ZnONP in ethanolic solutions of betulin and BDP (Fig. 8, *b*). Dispersions of zinc oxide nanoparticles in the starting ethanolic solutions and with immobilized triterpenoids, specifically, ZnONP—BDP and ZnONP—B, demonstrated strong blue-violet emission in the range 465—420 nm, caused by exciton radiation in the near zone. A distinction of the fluorescence spectra of ZnONP—B is the appearance of green-blue fluorescence in the range 470—480 nm.

The theoretically calculated range of emission wavelengths according to the published results[59] was 380—410 nm

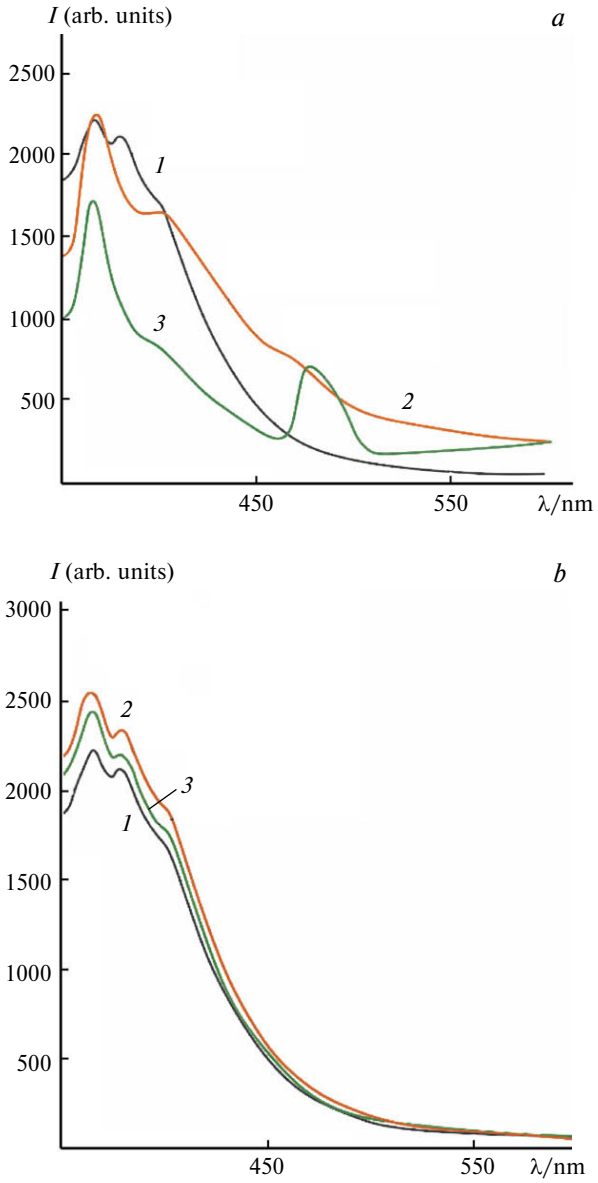

Fig. 8. *a*, Fluorescence spectra of ethanolic solutions of the starting ZnONP nanoparticles (*1*) and particles with immobilized triterpenoids ZnONP—BDP (*2*) and ZnONP—B (*3*); *b*, spectra of ZnONP dispersions (C_{ZnONP} = 0.33 mmol L^{-1}) (*1*) in 5 *M* ethanolic solutions of BDP (*2*) and betulin (*3*).

for the violet region and 435—593 nm for the blue and green regions.

A similar blue-violet emission of zinc oxide nanoparticles (λ_{em} = 411 nm for λ_{ex} = 320 nm) was described in a published work.[60] The authors explained this effect by a decrease in the density of oxygen vacancies due to the insertion of acetone, which is used as a solvent during synthesis. The immobilization of triterpenoids on the zinc oxide nanoparticle surface during modification is probably also related to the decrease in the density of crystal defects caused by oxygen. Fluorescence spectra with blue-violet emission in the range 360—400 nm were previously observed for zinc oxide nanoparticles obtained by the sol-gel method in the presence of triethanolamine in zinc acetate sol.[51]

The influence of the method of preparation of zinc oxide nanoparticles and the methods of their modification with triterpenoids on blue emission in fluorescence spectra can be explained using the results presented in the work.[59] The authors demonstrated the correspondence of the theoretically calculated Gaussian fluorescence spectra and the zinc oxide nanoparticle energy band diagrams obtained by various methods and in various media. The theoretical spectra were calculated taking into account the linewidth of each emission band (taking into account the shoulder and the unresolved bands), that is, 432, 382, 404, 412, 408, and 374 nm, respectively. It is believed that violet emission usually occurs due to interstitial zinc defects (Zn_i) during an electronic transition from defect Zn_i to the valence band, while blue emission is related to the transition from Zn_i to vacant defects.[56,61—63]

We assume that the presence of violet emission in the range 365—410 nm of the fluorescence spectrum of modified zinc oxide nanoparticles is probably due to a higher concentration of grains, dislocations, and surface traps appearing during the modification of the ZnO surface with triterpenoids (ZnONP—BDP and ZnONP—B).

In general, it should be noted that modified nanoparticles have a wurtzite crystal structure characterized by interstitial zinc defects (Zn_i). This is confirmed by the appearance of an absorption band in the UV spectrum due to exciton recombination (357—362 nm), and by the presence of blue-violet fluorescence in the range 380—410 nm. The surface concentration of BDP on ZnO nanoparticles was 100 mg g^{-1}, which makes it possible to use these modified particles as a component of lipophilic drugs due to the combined effect. This effect implies the manifestation of anti-inflammatory, wound-healing, and antitumor properties of BDP and antimicrobial and immunostimulating properties of zinc oxide nanoparticles.

Evaluation of the efficiency of ZnONP—BDP and betulin oleogel action on the healing of burn wounds in rats. Zinc oxide nanoparticles (5%) modified with an ethanolic solution of BDP were introduced into a 9% betulin oleogel in sunflower oil.

The treatment of a grade IIIb thermal contact burn in rats with the obtained composition for 10 days resulted in a more effective epithelialization of the skin on the wound compared to the control group (untreated burn, Fig. 9).

According to morphological studies, total necrosis with microabscesses without signs of regeneration was observed in the control group without treatment. In the group treated with betulin oleogel with zinc oxide nanoparticles modified by BDP, there was epithelialization at the edge of the wound with well-vascularized newly formed tissue without indications of edema with preserved capillarostasis and skin appendages. The behavior of animals (sleep, appetite, anxiety) and their condition (weight, fur, appearance, and area of the wound) after treatment with oleogel with nanoparticles was considerably better compared to control groups *1* and *3*. Biochemical parameters assessed using antioxidant enzyme activity demonstrated a high activity of the oleogel with nanoparticles (see Fig. 9).

An increase in the activity of superoxide dismutase, catalase, and glutathione reductase after 10 days of treat-

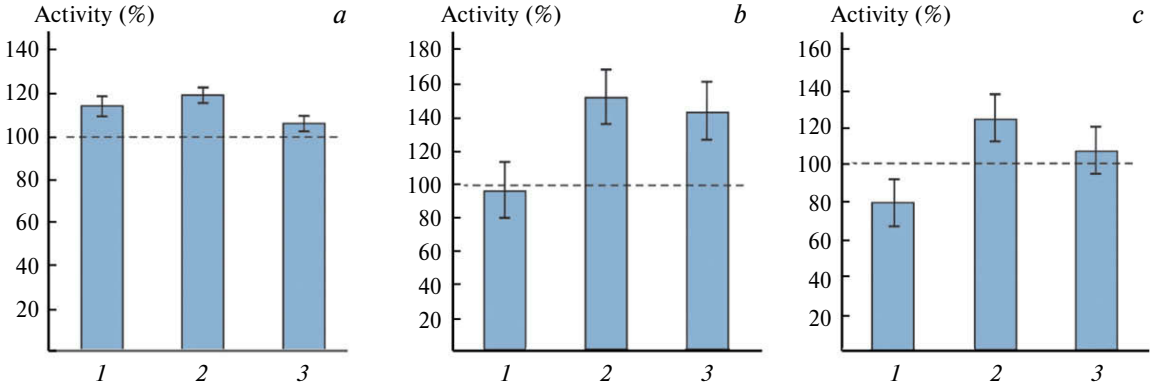

Fig. 9. Diagrams of the activity of enzymes (%) superoxide dismutase (*a*), catalase (*b*), and glutathione reductase (*c*) relative to the control group (untreated burn) taken as 100%: *1*, treatment with sunflower oil; *2*, treatment with oleogel with ZnONP—BDP and betulin; *3*, treatment with methyluracil ointment.

ment characterizes both the antioxidant properties of the obtained oleogel and the improved health of the animals in general. The wound-healing effect of the oleodispersion of betulin and zinc oxide nanoparticles is probably also caused by the beneficial effect of zinc ions, which is confirmed by numerous results on the positive effect of zinc compounds in the treatment of burns, including through the generation of active forms of oxygen, which have a bactericidal effect.[64—67] The generation of ROS was determined by the intensity of lipid peroxidation processes (an increase of 30% compared to control) and an increase in the level of malondialdehyde by 20—30% in *in vitro* experiments on white Wistar rat blood, stabilized with sodium citrate.

In conclusion, we demonstrated the formation of BDP—Zn^{2+} salt complexes at the BDP monolayer—aqueous solution of Zn^{2+} interface, which can be a convenient method for immobilizing BDP on the surface of zinc oxide nanoparticles, excluding additional conjugation or modification of the nanoparticle surface. The preparation of BDP complexes with zinc ions on the ZnO nanoparticle surface made it possible to enhance the permeability of betulin diphosphate and other biologically active components on the example of betulin. Thus, zinc oxide nanoparticles dissolve in acidic lysosomes with the release of BDP and zinc cations.

These studies have shown that modified zinc oxide nanoparticles with a high surface concentration of BDP, while preserving the structure of wurtzite, exhibit blue-violet fluorescence, and, consequently, promote the generation of ROS, which leads to the apoptosis of bacteria or tumor cells. This technique of immobilizing BDP with a high therapeutic potential on the surface of zinc oxide nanoparticles can be useful for the development of new drugs with anti-inflammatory, wound-healing, antitumor, antimicrobial, and immunostimulating effects.

This work was financially supported by the Ministry of Higher Education and Science of the Russian Federation within the basic part of the Russian state assignment (Project No. 0729-2020-0039).

References

1. G. A. Tolstikov, O. B. Flekhter, E. E. Shultz, L. A. Baltina, A. G. Tolstikov, *Chemistry for Sustainable Development*, 2005, **13**, 1.
2. D.-M. Zhang, H.-G. Xu, L. Wang, Y.-J. Li, P.-H. Sun, X.-M. Wu, G.-J. Wang, W.-M. Chen, W.-C. Ye, *Med. Res. Rev.*, 2015, **35**, 1127.
3. M. Chudzik, I. Korzonek-Szlacheta, W. Król, *Molecules*, 2015, **20**, 1610.
4. A. A. Damle, Y. P. Pawar, A. A. Narkar, *Indian J. Exp. Biol.*, 2013, **51**, 485.
5. A. Spivak, R. Khalitova, D. Nedopekina, L. Dzhemileva, M. Yunusbaeva, V. Odinokov, V. D´yakonov, U. Dzhemilev, *Molecules*, 2018, **23**, 3000.
6. F. B. Mullauer, L. van Bloois, J. B. Daalhuisen, M. S. Ten Brink, G. Storm, J. P. Medema, R. M. Schiffelers, J. H. Kessler, *Anticancer Drugs*, 2011, **22**, 223.
7. A. Halder, D. Shukla, S. Das, P. Roy, A. Mukherjee, B. Saha, *Cytokine*, 2018, **110**, 412.
8. E. A. Lomkova, P. Chytil, O. Janoušková, T. Mueller, H. Lucas, S. K. Filippov, O. Trhlíková, P. A. Aleshunin, Y. A. Skorik, K. Ulbrich, T. Etrych, *Biomacromolecules*, 2016, **17**, 3493.
9. S. K. Filippov, N. S. Vishnevetskaya, B.-J. Niebuur, E. Koziolová, E. A. Lomkova, P. Chytil, T. Etrych, C. M. Papadakis, *Colloid Polym. Sci.*, 2017, **295**, 1313.
10. O. V. Popova, V. V. Sursyakova, G. V. Burmakina, V. A. Levdansky, A. I. Rubaylo, *Dokl. Chem.*, 2015, **461**, 67.
11. A. Falamaş, S. C. Pînzaru, V. Chiş, C. Dehelean, *J. Mol. Struct.*, 2011, **993**, 297.
12. C. Şoica, C. Dehelean, C. Danciu, H. Wang, G. Wenz, R. Ambrus, F. Bojin, M. Anghel, *Int. J. Mol. Sci.*, 2012, **13**, 14992.
13. H. M. Wang, C. Soica, G. Wenz, *Nat. Prod. Commun.*, 2012, **7**, 289.
14. C. A. Dehelean, C. Soica, C. Peev, S. Ciurlea, S. Feflea, P. Kasa, *Farmacia*, 2009, **59**, 51.
15. U. Pradere, E. C. Garnier-Amblard, S. J. Coats, F. Amblard, R. F. Schinazi, *Chem. Rev.*, 2014, **114**, 9154.
16. D. V. Ponomaryov, L. R. Grigor´eva, A. V. Nemtarev, O. V. Tsepaeva, V. F. Mironov, I. S. Antipin, *Russ. Chem. Bull.*, 2020, **69**, 487.
17. H. X. Hao, J. K. Wang, Y. L. Wang, *J. Chem. Eng. Data,* 2004, **49**, 1697.
18. O. Vorobyova, O. Deryabina, D. Malygina, N. Plotnikova, A. Solovyeva, K. Belyaeva, N. Melnikova, *Sci. Pharm.*, 2018, **86**, 17.
19. N. B. Melnikova, D. S. Malygina, I. N. Klabukova, D. V. Belov, V. A. Vasin, P. S. Petrov, A. V. Knyazev, A. V. Markin, *Molecules*, 2018, **23**(5), 1175.
20. N. B. Melnikova, D. S. Malygina, O. N. Solovyeva, O. E. Zhiltsova, V. A. Vasin, P. S. Petrov, I. N. Klabukova, *Int. J. Pharm. Pharm. Sci.*, 2018, **10**, 87.
21. K.-N. Yu, T.-J. Yoon, A. Minai-Tehrani, J.-E. Kim, S. J. Park, M. S. Jeong, S.-W. Ha, J.-K. Lee, J. S. Kim, M.-H. Cho. *Toxicol. in Vitro*, 2013, **27**, 1187.
22. B. Ahmed, B. Solanki, A. Zaidi, M. S. Khan, J. Musarrat, *Toxicol. Res. (Camb.)*, 2019, **8**, 246.
23. L. Z. Flores-López, H. Espinoza-Gómez, R. J. Somanathan, *J. Appl. Toxicol.*, 2019, **39**(1), 16.
24. C. Danciu, I. Pinzaru, D. Coricovac, F. Andrica, I. Sizemore, C. Dehelean, F. Baderca, V. Lazureanu, C. Soica, M. Mioc, H. Radeke, *Eur. J. Pharm. Biopharm.*, 2019, **134**, 1.
25. M. Mioc, I.Z. Pavel, R. Ghiulai, D. E. Coricovac, C. Farcaş, C. V. Mihali, C. Oprean, V. Serafim, R. A. Popovici, C. A. Dehelean, M. I. Shtilman, A. M. Tsatsakis, C. Şoica, *Front. Pharmacol.*, 2018, **9**, 429.
26. B. Wang, W. Feng, M. Wang, Y. Gu, M. Zhu, H. Ouyang, J. Shi, F. Zhang, Y. Zhao, Z. Chai, H. Wang, J. Wang, *J. Nanopart. Res.*, 2008, **10**, 263.
27. V. Pokharkar, S. Dhar, D. Bhumkar, V. Mali, S. Bodhankar, B. L. Prasad. *J. Biomed. Nanotechnol.*, 2009, **5**, 233.

28. N. Thamer, L. Almashhedy. *Int. J. Phytopharm.*, 2016, **7**, 13.
29. M. Martínez-Carmona, Y. Gun´ko, M. Vallet-Regí, *Nanomaterials*, 2018, **8**, 268.
30. T. Jin, D. Sun, J. Y. Su, H. Zhang, H. J. Sue, *J. Food. Sci.*, 2009, 74, M46.
31. J.-S. Kim, B.-H. Kang, H.-M. Jeong, S.-W. Kim, B. Xu, *Curr. Appl. Phys.*, 2018, **18**, 681.
32. D. Bera, L. Qian, S. Sabui, S. Santra, P. H. Holloway, *Opt. Mater.*, 2008, **30**, 1233.
33. M. Uchiyama, M. Mihara, *Anal. Biochem.*, 1978, **86**, 271.
34. T. V. Sirota, *Biochemistry (Moscow)*, *Suppl. Ser. B: Biomed. Chem.*, 2011, **5**, 253.
35. H. Aebi, *Catalase in Vitro*, in *Methods in Enzymology*, Ed. L. Packer, Academic Press, Cambridge, MA, USA, 1984, Vol. **105**, pp. 121.
36. G. V. Sibgatullina, L. R. Khaertdinova, E. A. Gumerova, A. N. Akulov, Yu. A. Kostyukova, N. A. Nikonorova, N. I. Rumyantseva, *Metody opredeleniya redoks-statusa kul´tiviruyemykh kletok rasteniy. Uch.-metod. posob.* [*Methods for Determining the Redox State of Cultured Plant Cells. Ed. method. manual.*], Kazan. (Privolzhskii) fed. un-t, Kazan, 2011, 61 pp. (in Russian).
37. R. U. Khabriev, *Rukovodstvo po eksperimental´nomu (doklinicheskomu) izucheniyu novykh farmakologicheskikh veshchestv* [*Guidelines for Experimental (Pre-clinical) Study of New Pharmacological Substances*], Meditsina, Moscow, 2005, 832 pp. (in Russian).
38. R. Gennis, *Biomembranes: Molecular Structure and Functions*, Springer-Verlag, New York, 1989.
39. M. Broniatowski, M. Flasiński, P. Wydro, *Langmuir*, 2012, **28**, 5201.
40. D. Henrich, *Cryst. Growth Des.*, 2017, **17**, 5764.
41. M. Broniatowski, *J. Colloid Interface Sci.*, 2012, **381**, 116.
42. Y. Chen, R. Sun, B. Wang, *J. Colloid Interface Sci.*, 2011, **353**, 294.
43. P. Claesson, A. M. Carmona-Ribeiro, K. Kurihara. *J. Phys. Chem.*, 1989, **93**, 917.
44. M. Miller, M. Chu, B. Lin, M. Meron, P. Dutta. *Langmuir*, 2015, **32**, 73.
45. C. Yi. Kyunghee, Z. Horvolgyi, J. H. Fendler, *J. Phys. Chem.*, 1994, **98**, 3872.
46. G. Brezesinski, D. Vollhardt, *Chem. Phys. Chem.*, 2008, **9**, 1670.
47. E. V. Ermakova, I. N. Meshkov, Y. Y. Enakieva, A. I. Zvyagina, A. A. Ezhov, A. A. Mikhaylov, Y. G. Gorbunova, V. V. Chernyshev, M. A. Kalinina, V. V. Arslanov, *Surf. Sci.*, 2017, **660**, 39.
48. I. I. Shepeleva, A. V. Shokurov, N. V. Konovalova, V. V. Arslanov, P. A. Panchenko, S. L. Selektor, *Russ. Chem. Bull.*, 2018, **67**, 2159.
49. U. P. Rodrigues-Filho, S. Vaz, Jr, M. P. Felicissimo, M. Scarpellini, D. R. Cardoso, R. C. J. Vinhas, R. Landers, J. F. Schneider, B. R. McGarvey, M. L. Andersen, L. H. Skibsted, *J. Inorg. Biochem.*, 2005, **99**, 1973.
50. N. A. Vorob´yeva, Ph. D. Thesis (Chem.), Lomonosov Moscow State University, Moscow, 2015, 180 pp. (in Russian).
51. C. Wöll, *Prog. Surf. Sci.*, 2007, **82**, 55.
52. P. Bindu, S. Thomas. *J. Theor. Appl. Phys.*, 2014, **8**, 123.
53. B. Efafi, S. Ghamsari, M. A. Aberoumand, M. H. Majles Ara, H. Hojati Rad, *Mater. Lett.*, 2013, **111**, 78.
54. A. V. Blinov, A. A. Kravtsov, M. A. Yasnaya, A. Yu. Rusanov, E. V. Momot, *Mezhvuz. sb. "Fiziko-khimicheskie aspekty izucheniya klasterov, nanostruktur i nanomaterialov"* [*Interuniv. Coll. Vol. "Physicochemical Aspects of the Study of Clusters, Nanostructures, and Nanomaterials"*], 2015, **7**, 123 pp. (in Russian).
55. T. Thirugnanam, *J. Nanomater.*, 2013, **6**, 1
56. J. Oliva, L. Diaz-Torres, A. Torres-Castro, P. Salas, L. Perez-Mayen, E. De la Rosa, *Opt. Mater. Express*, 2015, **5**, 1109.
57. N. A. Salahuddin, M. El-Kemary, E. M. Ibrahim, *Nanoscience and Nanotechnology*, 2015, **5**, 82.
58. A. S. Lanje, S. K. Sharma, R. S. Ningthoujam, J.-S. Ahn, B. P. Ramchandra, *Adv. Powder Technol.*, 2013, **24**, 331.
59. L. K. Jangir, Y. Kumari, A. Kumar, M. Kumar, K. Awasthi, *Mater. Chem. Front.*, 2017, **1**, 1413.
60. B. Efafi, M. H. A. Majles, S. S. Mousavi, *J. Lumin.*, 2016, **178**, 384.
61. M. Vafee, M. S. Ghamsari, S. Radiman, *J. Lumin.*, 2011, **131**, 155.
62. M. Salavati-Niasari, F. Davar, A. Khansari, *J. Alloys Compd.*, 2011, **509**, 61.
63. Z. Chen, X. X. Li, G. Du, N. Chen, A. Y. M. Suen, *J. Lumin.*, 2011, **131**, 2072.
64. N. Abdulrahman, Z. Nssaif, *Tikrit J. Pure Sci.*, 2016, **21**, 49.
65. H. Hemeg, *Int. J. Nanomedicine*, 2017, **12**, 8211.
66. M. J. Hajipour, K. M. Fromm, A. A. Ashkarran, D. J. de Aberasturi, I. R. de Larramendi, T. Rojo, V. Serpooshan, W. J. Parak, M. Mahmoudi, *Trends Biotechnol.*, 2012, **30**, 499.
67. C. Han, N. Romero, S. Fischer, J. Dookran, A. Berger, A. Doiron, *Nanotechnol. Rev.*, 2017, **6**(5), 383; DOI: 10.1515/ntrev-2016-0054.

Received July 6, 2020;
in revised form August 31, 2020;
accepted October 1, 2020